Bactericidal Type IV Secretion System Homeostasis in Xanthomonas citri

William Cenens[1], Maxuel O. Andrade[2] and Chuck S. Farah[1]

Affiliations: [1]Departamento de Bioquímica, Instituto de Química, Universidade de São Paulo (USP), São Paulo, SP, Brazil. [2]Citrus Research and Education Center (CREC), Department of Microbiology and Cell Science, University of Florida, Lake Alfred, FL 33850, USA.

Contact: w.cenens@gmail.com and chsfarah@iq.usp.br

Abstract

Several *Xanthomonas* species have a type IV secretion system (T4SS) that injects a cocktail of antibacterial proteins into neighbouring Gram-negative bacteria, often leading to rapid lysis upon cell contact. This capability represents an obvious fitness benefit since it can eliminate competition while the liberated contents of the lysed bacteria could provide an increase in the local availability of nutrients. However, the production of this Mega Dalton-sized T4SS, with over a hundred subunits, also imposes a significant metabolic cost. Here we show that the chromosomal *virB* operon, which encodes the entirety of structural genes of the T4SS in *X. citri*, is regulated by the global regulator CsrA. Relieving CsrA repression from the *virB* operon produced a greater number of T4SSs in the cell envelope and an increased efficiency in contact dependent lysis of target cells. However, this was also accompanied by a physiological cost leading to reduced fitness when in co-culture with wild-type *X. citri*. We show that T4SS production is constitutive despite being downregulated by CsrA. Cells subjected to a wide range of rich and poor growth conditions maintain a constant density of T4SSs in the cell envelope and concomitant interbacterial competitiveness. These results show that CsrA provides a constant though partial repression on the *virB* operon, independent of the tested growth conditions, in this way controlling T4SS-related costs while at the same time maintaining *X. citri*'s aggressive posture when confronted by competitors.

Key Words: Interbacterial competition, Type IV secretions systems, CsrA, Single-cell fluorescent microscopy

Importance

Xanthomonas citri is a member of a family of phytopathogenic bacteria that can cause substantial losses in crops. At different stages of the infection cycle, these cells will encounter other bacterial species with whom they will have to compete for space and nutrients. One mechanism which improves a cell´s chance to survive these encounters is a type IV secretion system that transfers a cocktail of antimicrobial effector proteins into other Gram-negative bacteria in a contact-dependent manner. Here, we show that this system is constitutively produced at a low basal level, even during low nutrient conditions, despite representing a significant metabolic burden to the cell. The conserved global regulator, CsrA, provides a constant, nutrient-independent, repression on the production T4SS components, thereby holding production costs to a minimum while at the same time ensuring *X. citri*'s competitiveness during encounters with bacterial rivals.

Introduction

Type IV secretion systems (T4SS) are large systems spanning both the inner and outer membrane of many Gram-negative bacterial species (Low et al. 2014). The best described functions of T4SSs are the delivery of the pTi plasmid of *Agrobacterium tumefaciens* (Vergunst et al. 2000; Gordon & Christie 2014), their crucial roles in bacterial conjugation (Ilangovan et al. 2015) and involvement in delivering virulence factors to mammalian cells by several pathogenic species (Dehio & Tsolis 2017). T4SSs are made up of over 100 subunits of 12 different proteins (VirB1 to VirB11 plus VirD4) with a total size of over 3 MDa each (Low et al. 2014). Maintaining and expressing large operons and producing the amino-acids required to assemble the proteins they encode present a significant investment in terms of energy and raw materials for a cell (Akashi & Gojobori 2002; Wagner 2005; Lynch & Marinov 2015). Given the high cost secretion systems would have on cell physiology, it is not surprising that their production is often restricted to specific conditions, where they will be most needed. For example, expression of the *Agrobacterium tumefaciens* T4SS is dependent on pH, monosaccharides, phosphate and specific phenolic compounds released by wounded plant tissue (Das & Pazour 1989; Lohrke et al. 2001; Winans 1990; Gao & Lynn 2005).

60 Similarly, plasmid-borne *tra* genes, encoding a T4SS and other components of the
61 conjugation machinery, are only produced during specific conditions and often only in a
62 small portion of the population (Koraimann & Wagner 2014). Other examples include the
63 *Brucella suis* T4SS produced inside acidic phagocytic vacuoles of macrophages (Boschiroli et
64 al. 2002) and the *Ehrlichia ruminantium* T4SS whose genes are induced during iron
65 starvation (Moumène et al. 2017). This strict environmentally-dependent regulation is also
66 common in other secretion systems; for example, the *Vibrio cholera* type VI secretion system
67 (T6SS) is induced during high cell densities on chitinous surfaces (Borgeaud et al. 2015), the
68 *Xanthomonas citri* T6SS is specifically induced in the presence of amoeba (Bayer-Santos et al.
69 2018) and the *Shigella flexneri* type III secretion system is tightly regulated by oxygen levels
70 (Marteyn et al. 2010).

71 *X. citri* is a phytopathogen that causes citrus canker, a disease which can lead to significant
72 losses in citrus fruit production (Ryan et al. 2011; Mansfield et al. 2012). Previously, our
73 group has characterized the interbacterial killing activity of a T4SS in *X. citri* and showed that
74 this strain actively transfers a cocktail of antibacterial effector proteins into neighbouring
75 Gram-negative cells in a contact-dependent manner (Souza et al. 2015; Sgro et al. 2019).
76 More recently, we also described the antibacterial killing of a similar T4SS with its unique
77 antibacterial effectors in the opportunistic pathogen *Stenotrophomonas maltophilia* (Bayer-
78 Santos et al. 2019). Despite the importance of T4SSs in interbacterial competition, little is
79 known concerning the regulation of these systems in Xanthomonadaceae.

80 Microarray data of an *X. citri* strain harbouring a mutation in the global regulator CsrA (also
81 called RsmA) indicated its involvement in the regulation of over a hundred genes, including
82 the *virB* operon that encodes the T4SS proteins VirB1-11 (Andrade et al. 2014). CsrA is a
83 pleiotropic regulator linked to the genetic changes during stationary phase growth, biofilm
84 formation, gluconeogenesis and virulence (Romeo & Babitzke 2018). CsrA acts by binding
85 specific mRNA loops in 5' untranslated regions containing the canonical 5'-GGA-3' motif (Liu
86 & Romeo 1997; Holmqvist et al. 2016). In some cases, these interactions stabilize the mRNA
87 leading to increased expression, as for example has been observed for the *hrpG* mRNA in *X.*
88 *citri* (Andrade et al. 2014). More often, these CsrA-binding loops encompass the ribosome
89 binding site, in which case binding of CsrA inhibits translation (Baker et al. 2002). Although
90 several other means of CsrA regulation exist (Romeo & Babitzke 2018), the majority of

91 interactions lead to a repression of protein production (Potts et al. 2017). CsrA is regulated
92 by two important small RNAs, CsrB and CsrC (in *E. coli*) or by RsmY and RsmZ (in *P.*
93 *aeruginosa*), which contain several high affinity CsrA binding loops that effectively titrate
94 CsrA (Weilbacher et al. 2003; Janssen et al. 2018). Production of these small RNAs in *E. coli* is
95 controlled by several regulatory pathways, including the BarA/UvrY two-component system
96 that responds to molecules such as formate and acetate, the catabolite repression pathway
97 mediated by cAMP-CRP and the stringent response governed by RelA and SpoT-mediated
98 production of (p)ppGpp (Romeo & Babitzke 2018). Furthermore, direct regulation of CsrA
99 copy numbers in *E. coli* is achieved by five different promoters using at least two different
100 sigma factors (Yakhnin et al. 2011).

101 *X. citri* CsrA is very similar to CsrA from *E. coli* and *P. aeruginosa* (>77% identical), albeit the *X.*
102 *citri* protein has a 9 residue C-terminal extension. Detailed knowledge of CsrA, its targets
103 and its regulation in Xanthomonas species is limited. For example, the identity or presence
104 of regulatory small RNAs is not known. Nonetheless, some studies have shown phenotypic
105 alterations in a CsrA deletion strain reminiscent with known CsrA phenotypes in *E. coli* and *P.*
106 *aeruginosa*, such as reduced virulence, increased biofilm formation and increased glycogen
107 production (Chao et al. 2008; Lu et al. 2012) and direct RNA binding studies have also
108 confirmed the affinity of CsrA in *X. citri* for the canonical 5'-GGA-3' motifs (Andrade et al.
109 2014).

110 In this work, we show that the CsrA protein of *X. citri* represses the *virB* operon and that
111 removal of CsrA repression has a measurable fitness cost. This repression is incomplete
112 however, and so production of the *virB* products continues at a controlled basal level,
113 maintaining a constant density of T4SSs in the cell envelope during different growth
114 conditions. We propose that CsrA, in concert with other unidentified regulatory factors
115 working on the *virB* operon, leads to a sustained and energetically affordable aggressive
116 posture that contributes to *X. citri* competiveness and survival.

117

118 # Results

119 ## CsrA regulates the virB operon by binding to the 5' UTR of virB7

120 Based on transcription start site analysis data for *Xanthomonas campestris* (Alkhateeb et al.
121 2016) and further observations made in the Sequence Read Archive for *X. campestris and X.*
122 *citri* (https://www.ncbi.nlm.nih.gov/sra), the *Xanthomonas vir* locus contains two main
123 transcription start sites (TSSs) (Figure 1a). The presence of these TSSs in *X. citri* was
124 confirmed by 5'RACE analysis (Supplemental Figure S1). The first TSS is located 303
125 nucleotides upstream of *virD4* and a second TSS is located 249 nucleotides upstream of the
126 *virB7* start codon (Figure 1a and Supplemental Figure S1). Both *virD4* and *virB7* contain large
127 upstream regions, with the upstream region of *virD4* most probably containing an open
128 reading frame expressing a conserved protein of unknown function. Although an open
129 reading frame can be detected in the region downstream of *virD4* and upstream of *virB7*
130 (nucleotide sequence shown in Figure 1a), it lacks a canonical ribosome binding site and its
131 translated product is of very low sequence complexity and is not conserved in the protein
132 databases. Since a list of CsrA regulated genes in *X. citri* from a microarray dataset included
133 several of the *virB* genes (Andrade et al. 2014) we further scrutinised the *virB* 5'UTR
134 (upstream of the virB7 start codon, from here on referred to as $5'UTR_{B7}$). This analysis
135 revealed several 5'-GGA-3' CsrA-binding motifs (Figure 1a) that could be CsrA binding sites
136 when present in a stable loop structure (Holmqvist et al. 2016). To test this hypothesis, a
137 transcriptional *msfgfp* (encoding for the monomeric super folder green fluorescent protein)
138 fusion was constructed downstream of the genomic copy of *virB11* (*X. citri virB11-msfgfp*).
139 Single cell fluorescence analysis showed that upon deleting *csrA* in *X. citri virB11-msfgfp,*
140 msfGFP production from the *virB* operon is upregulated 3.3-fold (Figure 1b). In order to
141 confirm the direct regulation of CsrA on the $5'UTR_{B7}$, the $5'UTR_{B7}$ was cloned in between the
142 P_{tac} promotor (constitutive in the *lac* negative *X. citri* strain) and *msfgfp,* after which a single
143 copy of this construct was integrated into the α-amylase gene (*amy; xac0798*) in both the *X.*
144 *citri* wild-type and Δ*csrA* strain. The resulting fluorescence levels in the presence or absence
145 of CsrA shows that CsrA is capable of repressing msfGFP production from the P_{tac} promoter
146 when the $5'UTR_{B7}$ is present (Figure 1c). This indicates that the effect of CsrA is independent
147 of the *virB* promoter. Expanding these observations, we replaced the entire structural
148 operon (Figure 1a) by *msfgfp,* with the *msfgfp* start codon in the exact position of the *virB7*

149 start codon (*X. citri ΔvirB::P_{B7}-msfgfp*). Deleting *csrA* in this strain indeed showed a similar
150 response of increased msfGFP production from the *virB* operon (Figure 1d). Importantly, the
151 removal of the *5'UTR_{B7}* in this strain (*X. citri ΔvirB::P_{B7}-Δ5'UTR_{B7}-msfgfp*) caused msfGFP
152 levels to increase in the wild-type strain (Figure 1d). This increase in msfGFP production in
153 the absence of *5'UTR_{B7}* was only slightly lower than those observed in the *X. citri ΔvirB::P_{B7}-*
154 *msfgfp ΔcsrA* and *X. citri ΔvirB::P_{B7}-Δ5'UTR_{B7}-msfgfp ΔcsrA* strains, further confirming CsrA
155 regulation mediated by the 5'UTR_{B7}. We note that the *ΔcsrA* background has an elaborate
156 effect on *X. citri* physiology (for instance, cultures display an intense flocculation and
157 decreased cell-sizes) and that this could account for the subtle differences in msfGFP
158 production observed between strains lacking *csrA* with or without the *5'UTR_{B7}* in Figure 1d.
159 Next, the construction of a genomic deletion of the *5'UTR_{B7}*, while keeping all other *virB*
160 genes intact, resulted in a 3.9-fold increase in expression levels in the *X. citri Δ5'UTR_{B7}*
161 *virB11-msfgfp* reporter strain (Figure 2a). Finally, an electrophoretic mobility shift assay
162 (EMSA) confirmed the direct *in vitro* binding of CsrA to the *5'-UTR_{B7}* (Figure 1e). This result,
163 combined with all the gene expression data obtained from several different constructs
164 (Figures 1b to 1d and 2a) indicate that CsrA regulates *virB* operon expression by binding to
165 the *5'UTR_{B7}*, most probably by preventing translation and/or destabilizing the *virB*
166 transcripts.

167

168 Removal of CsrA repression on the virB operon increases T4SS numbers and bacterial killing.
169 Having established the direct role of CsrA in the repression of the *virB* operon, we asked
170 whether the interbacterial killing efficiency of *X. citri* would be enhanced in a strain lacking
171 the *5'UTR*$_{B7}$. We used a *X. citri virB10-msfgfp*$_{TL}$ translational fusion strain (Sgro et al. 2018) in
172 order to assess the number of T4SSs that are present per cell (see Materials and Methods
173 and Figure 2b). In this strain, the periplasmic VirB10 component has been replaced by a
174 VirB10-msfGFP chimera. Since each T4SS contains 14 copies of VirB10, assembled T4SSs can
175 be observed as fluorescent periplasmic foci and counted (Sgro et al. 2018). Deleting the
176 *5'UTR*$_{B7}$ in the *X. citri virB10-msfgfp*$_{TL}$ genetic background resulted in a 2.6-fold increase in
177 the number of fluorescent T4SS foci that were counted per cell (Figure 2b). We note that the
178 higher density of T4SSs in this strain leads to a more crowded periplasm, making it more
179 difficult to clearly separate individual foci, leading to an underestimation of total number of
180 T4SSs. Therefore, the calculated 2.6-fold increase should be considered a lower limit. As
181 could be expected, a higher number of T4SSs also increased the efficiency with which *X. citri*
182 lyses *E. coli* cells in a quantitative LacZ mediated CPRG-cleavage assay (Figure 2c). Using the
183 slopes of the curves in the CPRG-cleavage assays as a measure of killing efficiency (see
184 Materials and Methods), the *Δ5'UTR*$_{B7}$ strain kills 2.14-fold more efficiently than the *X. citri*
185 wild-type strain under these conditions (Figure 2c). However, these results also show that
186 under these conditions, removal of CsrA repression was not necessary to observe T4SS
187 dependent *E. coli* lysis in the CPRG assays (Figure 2c). This is in agreement with previously
188 published spot assays and CFU-based competition assays, all performed with wild type *X.*
189 *citri* strains (Souza et al. 2015). To test whether we could identify conditions in which T4SS-
190 mediated killing would be inhibited or enhanced, we tested *E. coli* lysis efficiencies at 18°C or
191 28°C, at pH 6, 7 and 8, in absence of Fe^{3+} and using different carbon sources (glucose,
192 sucrose or starch; Figure 2d). All the tested conditions led to clearly detectable T4SS
193 dependent lysis of *E. coli* cells with only small variations (+/- 35%) in killing efficiencies
194 (Figure 2d). Taken together, these observations indicate that the observed levels of msfGFP
195 signal from the *X. citri virB11-msfgfp* reporter strain (Figure 1b, 1d and 2a) and the discrete
196 numbers of T4SSs in the cell envelope (Figure 2b) present in the wild-type background,
197 represent the baseline expression and production levels of T4SS components and that these
198 levels, all repressed from what they would otherwise be in the absence of CsrA, are
199 sufficient to maintain T4SS production and efficient lysis of neighbouring target cells.

200

201 ## T4SS dependent interbacterial killing is maintained during growth under scarce nutrient
202 conditions

203 Considering the expected high energetic cost of producing T4SSs and the previously
204 described responsiveness of *csrA* regulons to nutrient input (Romeo & Babitzke 2018), we
205 decided to test whether lowering the nutrient contents of the growth media would change
206 T4SS-dependent killing efficiencies. To accomplish this, *X. citri* cultures were passed to media
207 containing normal or reduced levels of sucrose and/or casamino acids (the only nutrient
208 sources present in the defined media) and grown overnight plus an additional 9 hours in
209 fresh media for each culture to fully adapt to the conditions (see Materials and Methods for
210 details). These cultures were then subjected to a quantitative CPRG-cleavage assay under
211 standardized conditions. Figure 2e shows that *X. citri* grown in nutrient-scarce culture media
212 continues to sustain T4SS-dependent lysis of *E. coli* cells. *X. citri* cultures with limited access
213 to sucrose have slightly reduced killing efficiencies (23% decrease) while cells with limited
214 access to both casamino acids and sucrose presented slightly elevated (39% increase) killing
215 efficiencies (Figure 2e). Supplementary Movie S1 presents a time-lapse video of a mixed
216 culture of *X. citri* and *E. coli* cells growing in casamino acid-depleted media for over 30 hours
217 in which many events of *E. coli* cell lysis are observed upon contact with *X. citri* cells. For
218 comparison, Supplementary Movie S2 presents *X. citri* killing *E. coli* cells growing under
219 standard nutrient concentrations and also shows clear cell lysis upon contact with *X. citri*
220 cells. No *E. coli* lysis is observed in these experiments when T4SS-deficient *X. citri* strains are
221 employed ((Souza et al. 2015) and data not shown).

222

223

224

225 ## Constant but incomplete CsrA-mediated repression of the virB operon during different
226 growth conditions

227 Figures 2a and 2b, showed that removing the *5'UTR*$_{B7}$ leads to both increased msfGFP
228 production and T4SS assembly. In order to test how CsrA regulation impacts protein
229 production from the *virB* operon, we decided to look more closely at VirB production in the
230 presence and absence of the *5'UTR*$_{B7}$ under different growth conditions. To do this, we
231 began by comparing cytoplasmic msfGFP production from *X. citri virB11-msfgfp* and *X. citri*
232 *Δ5'UTR*$_{B7}$ *virB11-msfgfp* strains. Both strains were grown simultaneously in media with
233 sucrose, glucose, glycerol or starch as carbon sources or in media depleted for casamino
234 acids and/or sucrose. Cultures were grown overnight in the different media and after
235 diluting, grown for an additional 6 hours and msfGFP content was registered by
236 fluorescence microscopy.

237 Mean msfGFP production from the *X. citri virB11-msfgfp* strain remains fairly similar during
238 different inputs of carbohydrates and even in the absence of a carbohydrate source (Figure
239 3a; white boxplots). Reducing casamino acid concentrations, however, increases VirB
240 production 60% on average (both in combination with 0.2% or 0.01% sucrose). This increase
241 in expression levels seems to be independent of CsrA regulation since similar increases in
242 msfGFP production were detected when using the *X. citri Δ5'UTR*$_{B7}$ *virB11-msfgfp* strain
243 (Figure 3a, dark grey boxplots). In fact, when comparing the relative increases observed with
244 the removal of the *5'UTR*$_{B7}$, it appears that repression on the *5'UTR*$_{B7}$ leads to a reduction of
245 VirB protein production by, on average 3.8-fold (± 0.4) over all conditions tested for both
246 strains (Figure 3a, fold-changes are indicated above each pair of boxplots). As such, it
247 appears that CsrA represses the *virB* operon to an extent that is largely independent of the
248 carbon source or casamino acid availability.

249 ## Homeostasis of T4SS density in the cell envelope over a wide range of nutrient availability

250 Spurred by the increased expression of the *virB* operon during decreased inputs of casamino
251 acids, we set out to assess the number of assembled T4SS over a wide range of casamino
252 acid and sucrose concentrations. For this, an 8 by 8 matrix of wells containing defined media
253 with varying nutrients levels was created in a 96-well plate. With sucrose (rows) and
254 casamino acids (columns) ranging from 0.4% to 0.007% in a 1.8x dilution series. After 24
255 hours of growth and an additional 5 hours of growth after a 4-fold dilution in the same but

256 fresh media, *X. citri virB10-msfgfp*$_{TL}$ cells were sampled and immediately imaged by
257 fluorescence microscopy, registering both cell dimensions and the number of T4SS foci
258 present per cell. In total, 42 different conditions (Figure 3b inset) were sampled over two
259 separate experiments). Figures 3b and 3c show that the different nutritional inputs in each
260 well result in a range of cell sizes, represented by their average surface areas and reveal a
261 general trend of reduced cell size with reduced casamino acid or sucrose availability. Plotting
262 the number of T4SSs versus the surface area shows a linear increase in T4SS numbers with
263 increasing surface area (Figure 3d; Pearson correlation r = 0.34, as calculated for all data
264 points). However, this positive correlation in turn leads to an almost constant average T4SS
265 density (T4SS/surface area) in the cell envelope with a subtle increase observed for the
266 smallest cells (Figure 3d inset), in line with the observation of subtly increased msfGFP
267 production in the *X. citri virB11-msfGFP* transcriptional reporter at low casamino acid
268 concentrations (Figure 3a). These results also suggest that during the cell-cycle, when the
269 surface area gradually increases until cell division, T4SSs are added continuously. Therefore,
270 it seems that a *X. citri* population maintains the density of its T4SSs within a specific range
271 under a variety of nutritional conditions. The number of T4SSs relative to surface area (T4SS
272 density) could be an important factor in determining the probability that a *X. citri* cell is able
273 to successfully transfer effectors into a neighbouring target cell during interbacterial
274 competition.
275

276 T4SS overproduction in a Δ5'UTRB7 background has an impact on X. citri physiology and leads
277 to reduced growth speeds
278 Since *Δ5'UTR$_{B7}$* cells present a roughly 4-fold greater expression from the *virB* operon
279 (Figure 3a) and kills with approximately twice the efficiency as wild-type cells (Fig. 2c), we
280 asked whether this putative advantageous feature could be counter-balanced by the
281 inherent metabolic cost of T4SS production. We therefore set up a co-culture experiment to
282 test whether overproduction of T4SSs in the *Δ5'UTR$_{B7}$* background leads to a detectable
283 growth defect in *X. citri*. For this we took advantage of the difference in msfGFP production
284 levels between *X. citri virB11-msfgfp* and *X. citri Δ5'UTR$_{B7}$ virB11-msfgfp* (Figures 2a and 3a)
285 to sort wild type and overproduction cells by fluorescence microscopy. This mitigated the
286 need to introduce different antibiotic resistance markers in the genome that could on their
287 own lead to subtle physiological differences. Additionally, the strains used here are
288 genetically very closely related since they were obtained from the same recombination
289 events leading to either the wild-type or mutant *5'UTR$_{B7}$* allele (see Materials and Methods).
290 Separate cultures of different single colonies of each of the strains were synchronised in rich
291 AB media before being mixed and diluted in a 1:1 ratio into AB media supplemented with
292 0.2% sucrose and 0.01% casamino acids. Cultures were diluted regularly to avoid
293 saturatuion and fluorescence microscopy images of thousands of cells were obtained at
294 different time-points over a period of approximately one week. Figure 4a shows that the
295 *Δ5'UTR$_{B7}$* strain gets outpaced by the wild type *5'UTR$_{B7}$* strain leading. In two distinct
296 experiments using 3 or 4 separate cultures each, we observed a 19% and 13% average
297 decrease in the *X. citri Δ5'UTR$_{B7}$ virB11-msfgfp* cell population relative to the wild-type *X.*
298 *citri virB11-msfgfp* cell population (Figure 4a). Additionally, analysis of the cell sizes of the
299 two strains at several time points over a one week period revealed that the *Δ5'UTR$_{B7}$*
300 background consistently has a slightly larger surface area over volume ratio (SA/V; Figure
301 4b), indicative of smaller cell sizes. The SA/V ratio has been suggested to be a measure of
302 the physiological state of rod-shaped bacterial cells and is thought to be set by the
303 availability of nutrients (Harris & Theriot 2016; Harris & Theriot 2018). The observed
304 average size reduction (increase in SA/V) for *X. citri Δ5'UTR$_{B7}$ virB11-msfgfp* cells could be
305 attributed to the increased metabolic cost of nutrients consumed in T4SS production and/or
306 to stress induced by the greater number of T4SSs in the cell envelope. This experiment
307 reveals that T4SS production has a measurable cost and illustrates the importance of

308 balancing expenses with gains from increased aggressiveness during inter-bacterial
309 competition.
310

311 Discussion

312 We show here that the regulation of the *virB* operon in *X. citri*, coding for the structural
313 proteins of the T4SS, is under control of the global regulator CsrA which binds to sites in the
314 5' untranslated region of the polycistronic mRNA initiating at the *virB7* gene (*5'UTR*$_{B7}$; Figure
315 1). The removal of the *5'UTR*$_{B7}$ leads to an increase in production of *virB* encoded proteins,
316 which in turn leads to an increase in number of T4SSs present in the cell envelope and a
317 greater interbacterial killing efficiency (Figure 2a, 2b and 2c). Despite CsrA repression on the
318 *virB* operon, we have not yet found any growth condition that would greatly decrease nor
319 increase T4SS production and T4SS-dependent killing by wild-type *X. citri* cells (Figures 2d,
320 2e and 3a). Therefore, the removal of CsrA repression does not seem to be required to
321 induce production of the T4SS. Rather, CsrA repression maintains a discrete number of
322 T4SSs in the cell envelope over a range of different growth conditions tested (Figures 2 and
323 3).
324 Several factors can be imagined to influence the efficiency with which a *X. citri* cell can
325 mount a successful contact-dependent attack. Firstly, a T4SS needs to be present at the
326 contact interface between the attacking *X. citri* cell and the target rival cell. After a
327 successful contact, T4SS effectors need to be translocated through the T4SS. This is
328 dependent on both the availability of effectors and importantly, ATP to power the secretion.
329 For example, the subtle decrease in killing efficiencies in the sucrose-depleted conditions
330 (Figure 2e) might stem from reduced energy levels, since sucrose would be the main
331 carbohydrate fed into the glycolysis and citric acid metabolic pathways. Furthermore,
332 depleting nutrients also leads to much smaller cell sizes compared to the cells grown in rich
333 media (Harris & Theriot 2016). This reduction in cell size in itself could influence killing-
334 efficiencies by increasing the probability of small cells contacting larger *E. coli* cells when in
335 co-culture on a solid surface, since smaller, more spherical/less cylindrical *X. citri* cells will
336 have a more close-packed arrangement next to *E. coli* cells (Hudson 1949), increasing the
337 probabilities of successful T4SS contact. Expanding this line of reasoning, a unit mass of cells
338 formed during growth in reduced nutrient conditions would have a higher contact

339 probability as the same mass of cells formed during growth in rich conditions, because of
340 the former's greater number of single cells. Thus, the subtle increase in T4SS density with
341 lower nutrient inputs (Figure 3b) and the concomitant smaller cell sizes, could both be
342 responsible for the slight increases in killing efficiency in during growth in media depleted in
343 both casamino acids and sucrose (Figure 2e).
344 The complex regulatory features governing CsrA production and activity have been shown
345 to be orchestrated in response to a wide variety of signals (Yakhnin et al. 2011; Romeo &
346 Babitzke 2018). Complex regulation mechanisms, including negative autoregulation, have
347 been proposed to act to keep CsrA levels and activity relatively stable with greatly reduced
348 cell-to-cell variability, making CsrA an ideal regulator for homeostatic responses (Yakhnin et
349 al. 2011; Romeo & Babitzke 2018). Of note, an ancestral CsrA homolog has been shown to
350 act as a homeostatic control agent during flagella morphogenesis in the Gram positive
351 *Bacillus subtilis* (Mukherjee et al. 2011). As such, CsrA could integrate diverse signals that
352 relay information regarding the nutritional environment of the cell and subsequently
353 stabilise its own activity to ensure a constant regulatory effect on its target transcripts. In
354 light of this model of CsrA function, our experiments do indeed indicate that in *X. citri,* CsrA
355 acts to reduce production from the *virB* operon with roughly the same repressing power
356 over a wide range of growth conditions (Figure 3a). Recently, it was reported that CsrA
357 (RsmA) represses all three Type VI secretion systems in *Pseudomonas aeruginosa*, abolishing
358 translation under non-inducing conditions (Allsopp et al. 2017). Affinity of RNA loops for
359 CsrA can differ in several orders of magnitude (Duss et al. 2014) and so some CsrA-mRNA
360 associations will be very sensitive to fluctuations in mRNA levels and CsrA availability while
361 others remain insensitive. As such, CsrA–mRNA affinities could be tuned so as to
362 constitutively stabilise translation from one transcript at basal levels (such as for the *virB*
363 operon) and at the same time ensure that translation from other transcripts is only
364 derepressed by a specific trigger; for example by a specific condition that changes the
365 mRNA structure. Several genetic circuits leading to different outcomes are possible, but for
366 sake of general discussion, we note that it is unlikely that CsrA availability varies greatly
367 under different conditions, since this would be hard to reconcile with the simultaneous
368 control of the hundreds of transcripts through which CsrA exerts its pleiotropic effects
369 (Andrade et al. 2014; Potts et al. 2017).
370

371 The removal CsrA-based repression of T4SS production results in a two-fold increase in
372 interspecies bacteria killing efficiency (Figure 2c) which could be beneficial under certain
373 circumstances. However, the production of a T4SS has its costs: the maintenance and
374 transcription of an approximately 13 kb locus, multiple rounds of translation to produce the
375 over 100 subunits that need to be transported to the inner-membrane or periplasm and
376 assembled into a single system of over 3 MDa in size (Low et al. 2014). Since the
377 maintenance of a single gene and the production of the amino acids to build up its protein
378 product has a measurable cost (Akashi & Gojobori 2002; Wagner 2005; Lynch & Marinov
379 2015), it was not surprising that we were able detect a reduction in the fitness of the *X. citri*
380 strain in which CsrA-based repression was removed (Figure 4).

381 Inter-bacterial competition is increasingly being shown to be crucial for the fitness and
382 survival (Lories et al. 2017; García-Bayona & Comstock 2018) and structuring of bacterial
383 populations (Nadell et al. 2016) and possibly contributing to bacterial evolution by lysis and
384 subsequent uptake of DNA (Veening & Blokesch 2017). The continuous expression and
385 activity of the T4SS under different growth conditions, further illustrates the importance of
386 interbacterial killing and the benefits that are accompanied with it. The control of *X. citri*
387 T4SS production by CsrA, seems to guarantee constant levels of T4SSs that provide
388 protection against rival bacterial, but not too many to represent a metabolic burden, thus
389 maintaining a balance likely to be crucial for *X. citri* in the varied natural environments it
390 encounters during its life cycle, both within and outside of its plant host.

391

392 Materials and Methods

393 Bacterial strains, media and culturing.

394 All strains used are listed in Table S1. For all experiments, strains were grown in defined AB
395 media containing 15mM $(NH_4)_2SO_4$, 17mM Na_2HPO_4, 22mM KH_2PO_4, 50mM NaCl, 0.1 mM
396 $CaCl_2$, 1 mM $MgCl_2$ and 3 µM $FeCl_3$, at pH 7.0, supplemented with 10 µg/mL thiamine and 25
397 µg/mL uracil and varying concentrations of carbohydrate sources and casamino acids as
398 described in the text. For cloning purposes standard lysogeny broth (5g/l yeast, 5 g/l NaCl,
399 10 g/l tryptone and 15 g/l agar) and 2xYT (5 g/l yeast, 10 g/l NaCl, 16 g/l tryptone and 15 g/l
400 agar) were used. For counterselection, sucrose plates were used (5 g/l yeast, 10 g/l tryptone,

401 60 g/l sucrose). Standard incubations were performed at 28°C in 24-well plates using 1.5 ml
402 culture media or in 96-well plates with 200 µl culture media with shaking at 200 rpm. In
403 general, after a first overnight growth period in 2xYT medium, cells were transferred at a
404 100-fold dilution into AB defined media for a second overnight growth to synchronise
405 growth. Cells were then diluted in fresh media and, after 4- to 6-hour growth, imaged by
406 microscopy. In case of experiments involving different growth media compositions, cultures
407 were inoculated once more at a 100-fold dilution in the appropriate AB media composition
408 for overnight growth and a final re-inoculation in fresh media with dilutions ranging from 2-
409 fold to 100-fold, depending on the overnight attained optical densities. Note that cultures
410 grown under different nutrient conditions attained different densities after overnight growth.
411 Care was therefore taken to dilute each culture in its appropriate media such as to obtain
412 adequate numbers of cells for experimental assays but at the same time avoiding saturation
413 of the faster growing cultures. After a final 4- to 9-hour growth period cells were either
414 imaged with fluorescence microscopy or subjected to competition assays.

415 Cloning of constructs for genomic insertions and deletions.

416 All primers, plasmids and strains used for cloning and PCR verifications together with brief
417 description of the constructions are listed in Table 1. Genomic deletions and insertions in the
418 *X. citri* genome were all constructed using a two-step allelic exchange procedure (Hmelo et
419 al. 2015). For this, 500 to 1000 base pair-sized fragments up- and downstream from the
420 region of interest were amplified using a high-fidelity polymerase (Phusion, Thermo
421 Scientific) and cloned into the pNPTS138 vector either by traditional restriction digest
422 cloning (NEB and Thermo Scientific) or by Gibson assembly (NEB). The resulting plasmid was
423 used to transform the appropriate *X. citri* strain by electroporation (2.0 kV, 200 Ω, 25 µF, 0.2
424 cm cuvettes; Bio-Rad)(Sawitzke et al. 2011). A first recombination event was selected for on
425 LB plates containing 50 µg/ml kanamycin. Transformants were streaked for single colonies
426 on kanamycin plates whereafter several single colonies of the merodiploids (Kan^R, Suc^S)
427 were streaked on sucrose plates selecting for a second recombination event creating either a
428 wild-type or mutant allele. After confirmation of the loss of the kanamycin resistance
429 cassette together with *sacB*, a PCR was performed using primers that hybridize outside of
430 the homology regions to identify the target allele. Strains containing the wild type alleles
431 (revertants created at an equal rate during the second recombination event) were also

432 stored and used as controls for their respective mutants. For the insertion of the pPM7G
433 plasmid into the *amy* gene of *X. citri,* cells were electroporated with the pPM7G plasmid and
434 selected for on LB plates containing 50 µg/ml kanamycin. Integrity of the *virB* operon in
435 these strains was confirmed by PCR to exclude erroneous recombination with the pPM7G
436 cloned 5'UTR$_{B7}$ regions.

437 Chlorophenol red-β-D-galactopyranoside (CPRG) bacterial competition assay.

438 To visualize and quantify the ability of *X. citri* to lyse *E. coli* strain MG1655, a CPRG-based
439 method was used as described previously (Vettiger & Basler 2016; Sgro et al. 2018). Briefly,
440 to each well of a clear U-shaped bottom 96-well plate, 100 µL of a mixture of 0.5 X buffer A
441 (7.5mM $(NH_4)_2SO_4$, 8.5mM Na_2HPO_4, 11mM KH_2PO_4, 25mM NaCl, pH 7.0), 1.5% agarose and
442 40 µg/mL CPRG (Sigma-Aldrich) was added, and plates were thoroughly dried under a
443 laminar flow. *X. citri* cells grown in the appropriate media, were mixed in a 1:1 volume ratio
444 with a concentrated *E. coli* culture. The *E. coli* cultures were grown to OD_{600} = 1 in the
445 presence of 0.2 mM IPTG (inducing the *lac* operon) in 2XYT medium, washed once and
446 concentrated 10 times. Five microliters of *X. citri* and *E. coli* mixtures were immediately
447 added to the 96-well plate without puncturing or damaging the agarose, covered with a
448 transparent seal and quickly thereafter absorbance at 572 nm (A_{572}) was monitored over
449 time in a 96-well plate reader for at least 200 minutes (SpectraMax Paradigm, Molecular
450 Devices). The A_{572} values were processed using RStudio software (RStudio-Team 2016) and
451 plotted using the ggplot2 package (Wickham 2016). Background intensities obtained from
452 the mean of A_{572} values of non lysing *E. coli* cells were subtracted from the data series and
453 data were normalized for initial OD_{600} differences.

454 Fluorescence microscopy image acquisition and analysis.

455 Briefly, 1 µL of cell suspension was spotted on a thin agarose slab containing 1X buffer A
456 (15mM $(NH_4)_2SO_4$, 17mM Na_2HPO_4, 22mM KH_2PO_4, 50mM NaCl, pH 7) and 2% agarose and
457 covered with a #1.5 cover glass (Corning). For time-lapse imaging, thicker agar slabs
458 containing the appropriate media were constructed as described (Bayer-Santos et al. 2019).
459 Phase contrast and msfGFP emission images were obtained with a Leica DMI-8
460 epifluorescent microscope. msfGFP emissions were captured using 1000 to 1500 ms
461 exposure times at maximum excitation light intensities. The microscope was equipped with a
462 DFC365 FX camera (Leica), a HC PL APO 100x/1.4 Oil ph3 objective (Leica) and a GFP

463 excitation-emission band-pass filter cube (Ex.: 470/40, DC: 495, Em.: 525/50; Leica). For
464 detection of VirB10-msfGFP foci, eleven 0.05 µm Z-plane stacks were obtained from a 0.5
465 µm region within the centre of the cells. This allowed for a better signal to noise ratio of the
466 VirB10-msfGFP foci and increased detection of VirB10-msfGFP foci location in different
467 depths of the cell. These image stacks were background subtracted by a rolling ball
468 correction using a significant cell-free portion of each image as a reference and, finally,
469 combined by an average intensity projection using the FIJI software package (Schindelin et al.
470 2012). To obtain a quantitative representation of cell sizes, background corrected
471 fluorescence intensities and amount of foci present per cell, the images were analysed using
472 the MicrobeJ software package (Ducret et al. 2016).

473 ## Co-culture growth experiment

474 To illustrate the physiological burden associated with T4SS overexpression, four independent
475 *X. citri Δ5'UTR$_{B7}$ virB11-msfgp* mutants and four independent *X. citri virB11-msfgfp* strains
476 (revertants to wild-type from the second recombination even) were grown overnight in 2X
477 YT media, diluted 100-fold to defined AB media with 0.2% sucrose and 0.2% casamino acids
478 and grown overnight. These overnight cultures were mixed 1:1 and 10-fold diluted into fresh
479 AB media with 0.2% sucrose and 0.01% casamino acids. Immediately after mixing (at
480 timepoint 0h) fluorescence microscopy images were taken (as described above) to register
481 the exact ratio of *X. citri virB11-msfgfp* cells versus *X. citri Δ5'UTR$_{B7}$ virB11-msfgfp* cells. The
482 cultures were subsequently diluted regularly so to prevent cultures from reaching saturation
483 which would halt further cell division. At the indicated time-points several microscopy
484 images of each cultures were again acquired. Given that the *virB11-msfgfp* reporter in the
485 strain lacking the *5'UTR$_{B7}$* has a higher msfGFP production (histograms of the populations'
486 msfGFP fluorescence levels do not overlap), cells could be sorted by using average msfGFP
487 content and as such, an accurate quantification of the cell ratio between wild-type and
488 deleted *5'UTR$_{B7}$* strains could be calculated over time.

489 ## Transcription start site analysis

490 Transcriptional start sites of the *virD* and *virB* transcripts were obtained by using the 5' RACE
491 Kit (Roche), as described (Andrade et al. 2014). The oligos for *virD4* and *virB7* 5' RACE assays
492 are listed in Table S1. The resulting PCR fragments were blunt ligated into pGEM-T before
493 sequencing 3 independent clones, identifying the transcription start sites.

494 ### RNA electromobility shift assays

495 For the RNA electromobility shift assays, DNA fragments encoding either the entire 5' UTR
496 of the *virB* operon or a shortened fragment lacking the first 73 nucleotides (Δ1-73nt), were
497 amplified from *X. citri* genome using forward primers which include the T7 promoter
498 sequence (see Table S1). RNA transcripts of the cloned *5'UTR*$_{B7}$ fragments were produced *in*
499 *vitro* from the resulting purified PCR products by using the T7 Transcription kit (Roche) and
500 labeled by using the RNA 3' end biotinylation kit (Pierce). The CsrA recombinant protein was
501 purified as previously described (Andrade et al. 2014). Approximately 70 nM of purified CsrA
502 protein and 6.25 nM Biotin-labeled RNA were mixed with binding buffer [(10 mM HEPES pH
503 7.3, 20 mM KCl, 1mM MgCl2, 1 mM DTT, 5% glycerol, 0.1 µg/µL yeast tRNA, 20 U RNasin
504 (Promega)] in a total reaction volume of 20 µL. The binding reactions were incubated at
505 25°C for 20 min. A 5 µL aliquot of loading buffer (97% glycerol, 0.01% bromophenol blue,
506 0.01% xylene cyanol) was added to the binding reaction and immediately loaded and
507 resolved by 5% native polyacrylamide gels. The binding assays and detection of RNA
508 products were performed with the LightShift Chemiluminescent RNA EMSA Kit (Thermo
509 Scientific). For the control reactions, 312.5 nM competitor unlabeled RNA of the *virB*
510 *5'UTR*$_{B7}$ was added to the binding reactions.

511

512 ## Acknowledgments

513 We thank Alexandre Bruni-Cardoso for unlimited access to the Leica DMI8 microscope.
514 Special thanks to Ioannis Passaris and Sander K. Govers for very helpful discussions,
515 suggestions and critical reading of the manuscript, and to Gilberto Kaihami for the
516 introduction to the R programming language. This work was supported by a FAPESP post-
517 doctoral grant to William Cenens (2015/18237-2) and FAPESP research grants to Chuck
518 Shaker Farah (2011/07777-5 and 2017/17303-7).

519

520 ## References

521 Akashi, H. & Gojobori, T., 2002. Metabolic efficiency and amino acid composition in the
522 proteomes of Escherichia coli and Bacillus subtilis. *Proceedings of the National*

523 *Academy of Sciences*, 99(6), pp.3695–3700.
524 Alkhateeb, R.S. et al., 2016. Genome wide transcription start sites analysis of Xanthomonas
525 campestris pv. campestris B100 with insights into the gum gene cluster directing the
526 biosynthesis of the exopolysaccharide xanthan. *Journal of biotechnology*, 225, pp.18–
527 28.
528 Allsopp, L.P. et al., 2017. RsmA and AmrZ orchestrate the assembly of all three type VI
529 secretion systems in Pseudomonas aeruginosa. *Proceedings of the National Academy of*
530 *Sciences of the United States of America*, 114(29), pp.7707–7712.
531 Andrade, M.O., Farah, C.S. & Wang, N., 2014. The Post-transcriptional Regulator rsmA/csrA
532 Activates T3SS by Stabilizing the 5??? UTR of hrpG, the Master Regulator of hrp/hrc
533 Genes, in Xanthomonas W. Ma, ed. *PLoS Pathogens*, 10(2), p.e1003945.
534 Baker, C.S. et al., 2002. CsrA regulates glycogen biosynthesis by preventing translation of
535 glgC in Escherichia coli. *Molecular Microbiology*, 44(6), pp.1599–1610.
536 Bayer-Santos, E. et al., 2019. The opportunistic pathogen Stenotrophomonas maltophilia
537 utilizes a type IV secretion system for interbacterial killing. *bioRxiv*, p.557322.
538 Bayer-Santos, E. et al., 2018. Xanthomonas citri T6SS mediates resistance to Dictyostelium
539 predation and is regulated by an ECF σ factor and cognate Ser/Thr kinase.
540 *Environmental Microbiology*, 20(4), pp.1562–1575.
541 Borgeaud, S. et al., 2015. The type VI secretion system of Vibrio cholerae fosters horizontal
542 gene transfer. *Science*, 347(6217), pp.63–67.
543 Boschiroli, M.L. et al., 2002. The Brucella suis virB operon is induced intracellularly in
544 macrophages. *Proceedings of the National Academy of Sciences*, 99(3), pp.1544–1549.
545 Chao, N.-X. et al., 2008. The rsmA -like Gene rsmA Xcc of Xanthomonas campestris pv.
546 campestris Is Involved in the Control of Various Cellular Processes, Including
547 Pathogenesis . *Molecular Plant-Microbe Interactions*, 21(4), pp.411–423.
548 Das, A. & Pazour, P.J., 1989. Delineation of the regulatory region sequences of
549 Agrobacterium tumefaciens virB operon. *Nucleic Acids Research*, 17(12), pp.4541–
550 4550.
551 Dehio, C. & Tsolis, R.M., 2017. Type IV effector secretion and subversion of host functions by
552 bartonella and brucella species. In *Current Topics in Microbiology and Immunology*.
553 Springer, Cham, pp. 269–295.
554 Ducret, A., Quardokus, E.M. & Brun, Y. V., 2016. MicrobeJ, a tool for high throughput

555 bacterial cell detection and quantitative analysis. *Nature Microbiology*, 1(7), p.16077.
556 Duss, O. et al., 2014. Molecular basis for the wide range of affinity found in Csr/Rsm protein-
557 RNA recognition. *Nucleic Acids Research*, 42(8), pp.5332–5346.
558 Gao, R. & Lynn, D.G., 2005. Environmental pH sensing: Resolving the VirA/VirG two-
559 component system inputs for Agrobacterium pathogenesis. *Journal of Bacteriology*,
560 187(6), pp.2182–2189.
561 García-Bayona, L. & Comstock, L.E., 2018. Bacterial antagonism in host-associated microbial
562 communities. *Science*, 361(6408), p.eaat2456.
563 Gordon, J.E. & Christie, P.J., 2014. The Agrobacterium Ti Plasmids. *Microbiology Spectrum*,
564 2(6), pp.1–18.
565 Harris, L.K. & Theriot, J.A., 2016. Relative Rates of Surface and Volume Synthesis Set
566 Bacterial Cell Size. *Cell*, 165(6), pp.1479–1492.
567 Harris, L.K. & Theriot, J.A., 2018. Surface Area to Volume Ratio: A Natural Variable for
568 Bacterial Morphogenesis. *Trends in Microbiology*, 26(10), pp.815–832.
569 Hayashi, K. et al., 2006. Highly accurate genome sequences of Escherichia coli K-12 strains
570 MG1655 and W3110. *Molecular Systems Biology*, 2, p.2006.0007.
571 Hmelo, L.R. et al., 2015. Precision-engineering the Pseudomonas aeruginosa genome with
572 two-step allelic exchange. *Nature protocols*, 10(11), pp.1820–41.
573 Holmqvist, E. et al., 2016. Global RNA recognition patterns of post-transcriptional regulators
574 Hfq and CsrA revealed by UV crosslinking in vivo. *The EMBO journal*, 35(9),
575 p.e201593360.
576 Hudson, D.R., 1949. Density and Packing in an Aggregate of Mixed Spheres. *Journal of*
577 *Applied Physics*, 20(2), pp.154–162.
578 Ilangovan, A., Connery, S. & Waksman, G., 2015. Structural biology of the Gram-negative
579 bacterial conjugation systems. *Trends in microbiology*, 23(5), pp.301–310.
580 Janssen, K.H. et al., 2018. *Functional analyses of the RsmY and RsmZ small noncoding*
581 *regulatory RNAs in Pseudomonas aeruginosa*,
582 Ke, N. et al., 2016. Visualization of periplasmic and cytoplasmic proteins with a self-labeling
583 protein tag. *Journal of Bacteriology*, 198(7).
584 Koraimann, G. & Wagner, M.A., 2014. Social behavior and decision making in bacterial
585 conjugation. *Frontiers in Cellular and Infection Microbiology*, 4(April), pp.1–7.
586 Liu, M.Y. & Romeo, T., 1997. The global regulator CsrA of Escherichia coli is a specific mRNA-

587 binding protein. *Journal of bacteriology*, 179(14), pp.4639–42.
588 Lohrke, S.M., Yang, H. & Jin, S., 2001. Reconstitution of Acetosyringone-mediated
589 Agrobacterium tumefaciens virulence gene expression in the heterologous host
590 Escherichia coli. *Journal of Bacteriology*, 183(12), pp.3704–3711.
591 Lories, B. et al., 2017. Meeting report on the ASM Conference on Mechanisms of
592 Interbacterial Cooperation and Competition. *Journal of Bacteriology*, p.JB.00403-17.
593 Low, H.H. et al., 2014. Structure of a type IV secretion system. *Nature*, 508(7497), pp.550–
594 553.
595 Lu, X.H. et al., 2012. RsmA Regulates Biofilm Formation in Xanthomonas campestris through
596 a Regulatory Network Involving Cyclic di-GMP and the Clp Transcription Factor. *PLoS*
597 *ONE*, 7(12), pp.1–11.
598 Lynch, M. & Marinov, G.K., 2015. The bioenergetic costs of a gene. *Proceedings of the*
599 *National Academy of Sciences*, 112(51), p.201514974.
600 Mansfield, J. et al., 2012. Top 10 plant pathogenic bacteria in molecular plant pathology.
601 *Mol Plant Pathol*, 13(6), pp.614–629.
602 Marteyn, B. et al., 2010. Modulation of Shigella virulence in response to available oxygen in
603 vivo. *Nature*, 465(7296), pp.355–358.
604 Martins, P.M.M. et al., 2010. Subcellular localization of proteins labeled with GFP in
605 Xanthomonas citri ssp. citri: Targeting the division septum. *FEMS Microbiology Letters*,
606 310(1), pp.76–83.
607 Moumène, A. et al., 2017. Iron Starvation Conditions Upregulate Ehrlichia ruminantium
608 Type IV Secretion System, tr1 Transcription Factor and map1 Genes Family through the
609 Master Regulatory Protein ErxR. *Frontiers in Cellular and Infection Microbiology*, 7,
610 p.535.
611 Mukherjee, S. et al., 2011. CsrA-FliW interaction governs flagellin homeostasis and a
612 checkpoint on flagellar morphogenesis in Bacillus subtilis. *Molecular Microbiology*,
613 82(2), pp.447–461.
614 Nadell, C.D., Drescher, K. & Foster, K.R., 2016. Spatial structure, cooperation and
615 competition in biofilms. *Nature Reviews Microbiology*, 14(9), pp.589–600.
616 Potts, A.H. et al., 2017. Global role of the bacterial post-transcriptional regulator CsrA
617 revealed by integrated transcriptomics. *Nature Communications*, 8(1), p.1596.
618 Romeo, T. & Babitzke, P., 2018. Global Regulation by CsrA and Its RNA Antagonists.

619 *Microbiology Spectrum*, 6(2), pp.1–14.
620 RStudio-Team, 2016. RStudio: Integrated Development for R. *RStudio, Inc., Boston, MA*.
621 Available at: http://www.rstudio.com/.
622 Ryan, R.P. et al., 2011. Pathogenomics of Xanthomonas: understanding bacterium–plant
623 interactions. *Nature Reviews Microbiology*, 9(5), pp.344–355.
624 Sawitzke, J.A. et al., 2011. Probing cellular processes with oligo-mediated recombination
625 and using the knowledge gained to optimize recombineering. *Journal of molecular*
626 *biology*, 407, pp.45–59.
627 Schindelin, J. et al., 2012. Fiji: An open-source platform for biological-image analysis. *Nature*
628 *Methods*, 9(7), pp.676–682.
629 Sgro, G.G. et al., 2019. Bacteria-killing Type IV Secretion Systems. *Frontiers in Microbiology*,
630 10, p.1078.
631 Sgro, G.G. et al., 2018. Cryo-EM structure of the bacteria-killing type IV secretion system
632 core complex from Xanthomonas citri. *Nature Microbiology*, p.1.
633 da Silva, A.C.R. et al., 2002. Comparison of the genomes of two Xanthomonas pathogens
634 with differing host specificities. *Nature*, 417(6887), pp.459–463.
635 Souza, D.P. et al., 2015. Bacterial killing via a type IV secretion system. *Nature*
636 *Communications*, 6, pp.1–9.
637 Veening, J.-W. & Blokesch, M., 2017. Interbacterial predation as a strategy for DNA
638 acquisition in naturally competent bacteria. *Nature Reviews Microbiology*, 15(10),
639 pp.621–629.
640 Vergunst, A.C. et al., 2000. VirB / D4-Dependent Protein Translocation from Agrobacterium
641 into Plant Cells. *Science*, 290(November), pp.979–982.
642 Vettiger, A. & Basler, M., 2016. Type VI Secretion System Substrates Are Transferred and
643 Reused among Sister Cells. *Cell*, 167(1), p.99–110.e12.
644 Wagner, A., 2005. Energy constraints on the evolution of gene expression. *Molecular*
645 *Biology and Evolution*, 22(6), pp.1365–1374.
646 Weilbacher, T. et al., 2003. A novel sRNA component of the carbon storage regulatory
647 system of Escherichia coli. *Molecular Microbiology*, 48(3), pp.657–670.
648 Wickham, H., 2016. *ggplot2: Elegant Graphics for Data Analysis*, Springer-Verlag New York.
649 Winans, S.C., 1990. Transcriptional induction of an Agrobacterium regulatory gene at
650 tandem promoters by plant-released phenolic compounds, phosphate starvation, and

651 acidic growth media. *Journal of Bacteriology*, 172(5), pp.2433–2438.
652 Yakhnin, H. et al., 2011. Complex regulation of the global regulatory gene csrA: CsrA-
653 mediated translational repression, transcription from five promoters by Eσ70 and EσS,
654 and indirect transcriptional activation by CsrA. *Molecular microbiology*, 81(3), pp.689–
655 704.
656

657 Supplementary Files Legends

658 **Table S1:** Primers, strains and plasmids used in this study
659
660 **Figure S1:** 5'RACE assay identifying the transcription start sites for *virD4* and *virB7*. **a)**
661 bottom panel shows the two adjacent possible transcription start sites of *virD4* (red and
662 purple arrow) due to sequencing ambiguity. The possible start sites are indicated with a
663 purple G and a red C in the nucleotide sequence (top panel). *VirD4* sequence starts at the
664 end of the displayed nucleotide sequence. In between the TSS and *virD4* a putative ORF of
665 unknown function is present. **b)** Similar analysis for *virB7* with start site depicted with red
666 arrow (bottom panel) and red G in the nucleotide sequence (top panel). In panel a and b,
667 translation start sites are depicted in red and open reading frames in blue. In bold are the
668 putative polymerase binding sites and in underlined regular font the ribosome binding sites.
669
670 **Movie S1:** Time-lapse movie showing contact dependent lysis at the single cell level during
671 growth in media depleted for casamino acids. Movie starts after 25 hours of growth on the
672 pad. Clearly showing greatly decreased growth speeds. White arrows indicate regions were
673 *E. coli* cells come into contact with the smaller sized *X. citri* cells. Scalebar indicates 5µm.
674 Timestamp in bottom left of the movie.
675
676 **Movie S2:** Time-lapse movie showing contact dependent lysis at the single cell level during
677 growth in rich media. Movie was started and ran in parallel with Movie S1. Starting at
678 timepoint zero. White arrows indicate regions were *E. coli* cells come into contact with
679 smaller sized *X. citri* cells. Scalebar indicates 5µm. Timestamp in bottom left of the movie.
680
681

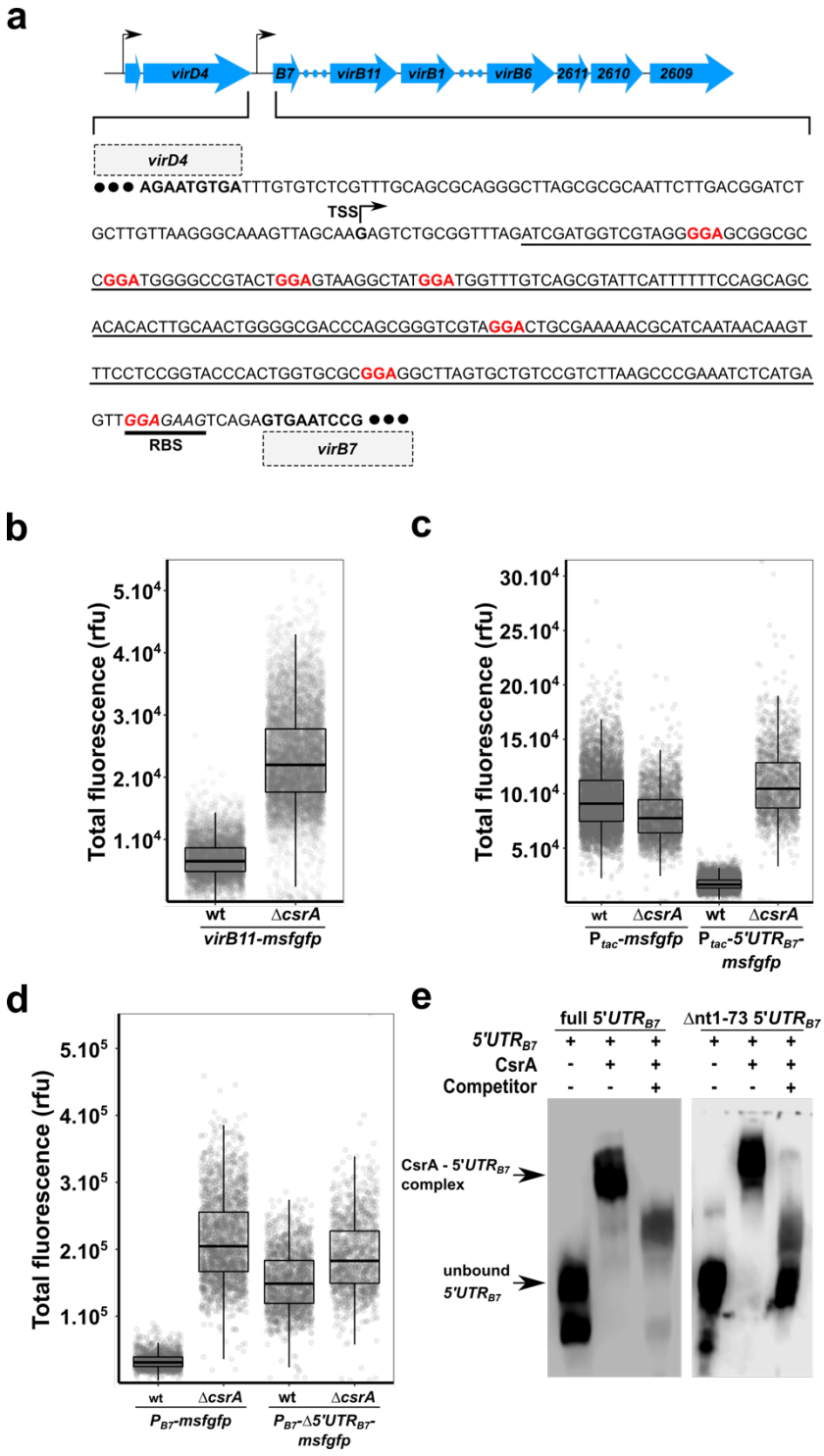

Figure 1: **CsrA regulates the *virB* operon. a)** An on-scale schematic of the *virD* and *virB* operons with black arrows indicating positions of the transcription start sites, blue arrows indicating the open reading frames and blue dots representing genes not shown. The intergenic sequence between *virD4* and *virB7* genes is shown and the *virB7* transcription start site (TSS) is indicated. The 5'-GGA-3' motifs are indicated in red and the predicted ribosome binding site (RBS) is underlined with a thick black line. The sequence that is deleted in the *Δ5'UTR$_{B7}$* strains is underlined with a thin black line. **b)** Single cell msfGFP fluorescence levels of the *X. citri virB11-msfgfp* transcriptional reporter in *X. citri* wild type and *ΔcsrA* strains. Production of msfGFP increased on average 3.3-fold in the *ΔcsrA* strain (N_{wt} = 4887 cells and $N_{\Delta csrA}$ = 6263 cells, from a single representative culture each). **c)** Single cell msfGFP fluorescence levels of the *amy::P$_{tac}$-msfgfp* and

691 *amy::P_{tac}-5'UTR_{B7}-msfgfp* reporters in *X. citri* wild type and *ΔcsrA* strains. A CsrA-dependent reduction in msfGFP
692 production is only observed in the strain containing the *5'UTR_{B7}* (average 5.8-fold reduction, N_{wt} = 6862 cells and $N_{\Delta csrA}$ =
693 1671 cells, from 2 separate cultures each). The control lacking the *5'UTR_{B7}* in between the P_{tac} promotor and *msfgfp* (*X.citri*
694 *amy::P_{tac}-msfgfp*) showed no CsrA-dependent repression of msfGFP production (average 16% increase, N_{wt} = 5534 cells and
695 $N_{\Delta csrA}$ = 2495 cells, from 2 separate cultures each). **d)** Single cell msfGFP fluorescence levels of the *msfgfp* reporter that
696 substituted the entire structural *virB* operon (with the *msfgfp* start codon placed at the exact position of the *virB7* start
697 codon) in *X. citri* wild type and *ΔcsrA* strains with an intact *virB* promoter (*P_{B7}*) or a *virB* promoter in which the *5'UTR_{B7}* was
698 deleted (*P_{B7}-Δ5'UTR_{B7}*). *X. citri ΔvirB::P_{B7}-Δ5'UTR_{B7}-msfgfp* shows higher msfGFP production than the *X. citri ΔvirB::P_{B7}-*
699 *msfgfp* strain lacking the *5'UTR_{B7}* (average 6.5-fold increase, N_{wt} = 1495 cells and $N_{\Delta csrA}$ = 2156 cells, from 2 separate
700 cultures each). Absence of the *5'UTR_{B7}* almost completely abolishes CsrA dependent down-regulation of expression levels
701 (average 1.2-fold increase, N_{wt} = 1748 cells and $N_{\Delta csrA}$ = 1304 cells, from 2 separate cultures each). Note that removal of the
702 *5'UTR_{B7}* in the wild-type backgrounds led to a 4.6-fold increase. **e)** An electrophoresis mobility shift assay (EMSA) shows
703 direct *in vitro* binding of CsrA with the complete and a shortened fragment (lacking the first 73 nucleotides) of the *5'UTR_{B7}*.
704 Addition of unlabelled *5'UTR_{B7}* RNA competes with labelled DNA binding. Tukey box-and-whisker plots in parts b, c and d:
705 black central line (median), box (first and third quartiles) and whiskers (data within 1.5 interquartile range).

706

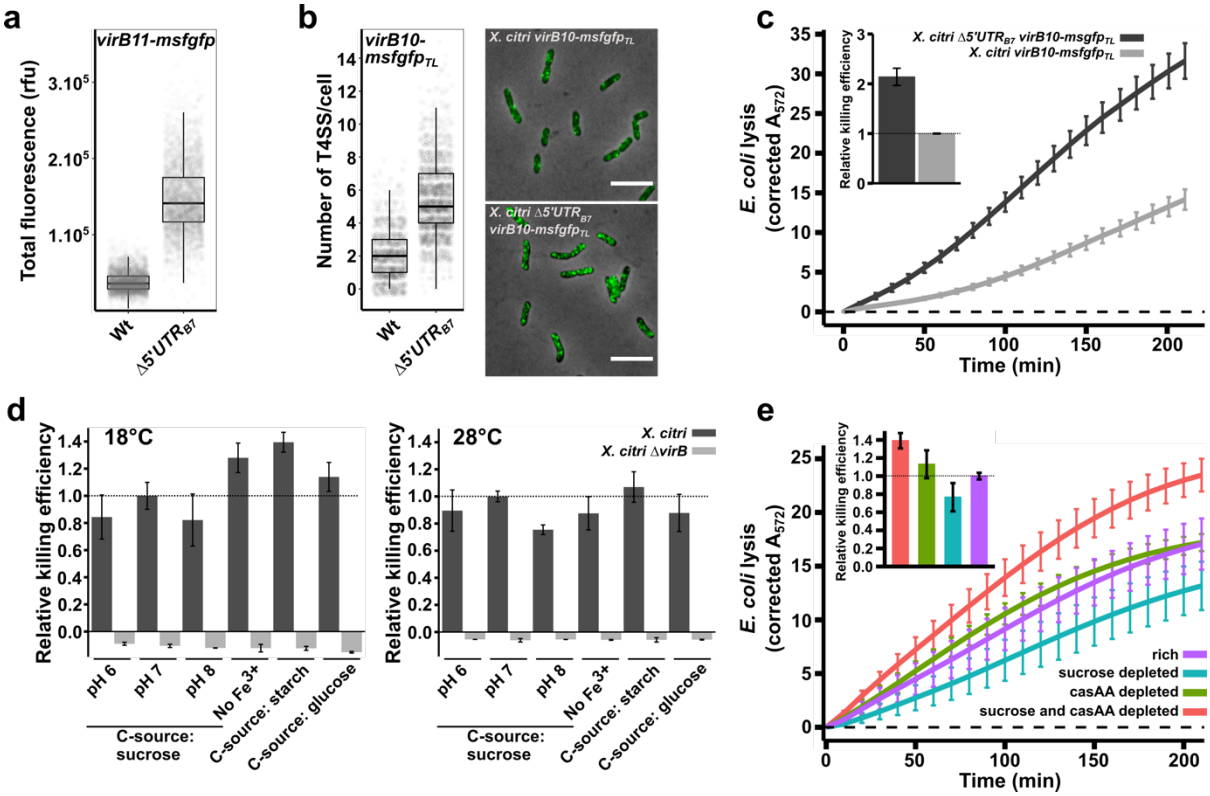

Figure 2: **VirB production and interbacterial killing is constitutive under incomplete repression by CsrA**. **a)** Single cell msfGFP fluorescence levels from the *X. citri virB11-msfgfp* reporter strain with and without the genomic deletion of the *5'UTR$_{B7}$* (underlined region in Figure 1a; *X. citri Δ5'UTR$_{B7}$ virB11-msfgfp*). Removing the *5'UTR$_{B7}$* leads to a 3.9-fold increase in msfGFP production from the *virB* operon (N_{wt} = 3397 cells and $N_{\Delta 5'UTR}$ = 3099 cells, from 4 separate cultures). **b)** Quantification of single fluorescent foci of T4SSs containing the VirB10-msfGFP chimera. The genomic deletion of the *5'UTR$_{B7}$* in the *X. citri virB10-msfgfp$_{TL}$* strain increased the number of T4SSs per cell 2.6-fold (N_{wt} = 1361 cells and $N_{\Delta 5'UTR}$ = 2062 cells, from 3 separate cultures). Note that the increased amount of T4SS in the *Δ5'UTR$_{B7}$* strain in some cases causes the VirB10-msfGFP produced fluorescent foci to overlap, limiting the separation of the single foci, leading to an underestimation of the number of T4SS per cell. **c)** Quantitative CPRG cleavage-based killing assay in the presence or absence of CsrA repression on the *virB* operon using the same *X. citri virB1-msfgfp$_{TL}$* and *X. citri Δ5'UTR$_{B7}$ virB10-msfgfp$_{TL}$* cultures analysed in part **b**. Genomic deletion of the *5'UTR$_{B7}$* leads to a 2.14-fold increase in lysis of *E. coli* cells. The inset shows the slope value of the linear part of the depicted curves relative to the wild-type strains (N = 4 separate cultures with 2 technical repeats each). **d)** Quantitative CPRG cleavage-based killing assays of wild type *X. citri* cells grown in different conditions (dark grey bars). Killing efficiencies were evaluated in defined media containing different carbon sources (0.2 % sucrose, 50 µg/ml starch or 0.2% glucose), pH 6, 7 and 8, lack of Fe^{3+} and at different temperatures (18°C and 28°C). Values represent the slope of the linear part of the OD_{572} curves as described in panel c and normalized relative to the condition at pH 7 (which is the condition used throughout the manuscript). As a control, killing efficiency of a T4SS-deficient mutant (*X. citri ΔvirB::P$_{B7}$-msfgfp*; light grey bar) was assessed after growth under the same conditions (N = 4 separate cultures with two technical repeats). **e)** Quantitative CPRG cleavage-based killing assays from *X. citri* cells grown at different nutrient levels. Killing efficiencies of wild type *X. citri* strains are maintained during growth in defined media containing either 0.2% or 0.01% sucrose and/or casamino acids (casAA). Inset shows the slope value of the linear part of the depicted curves relative to the killing curve from the *X. citri* cultures grown in rich media. Cultures reduced in both casamino acid and sucrose concentrations show a 39% increase whereas sucrose depleted cultures have a 23% reduction in efficiencies compared to the reference (N = 5 separate cultures with 4 technical repeats). Error bars in panels c, d and e

732 indicate the standard deviation. Horizontal dashed line in c and e represents the zero-line obtained after subtracting the
733 background signal of non-lysed *E. coli* cultures grown in parallel during each experiment.

734

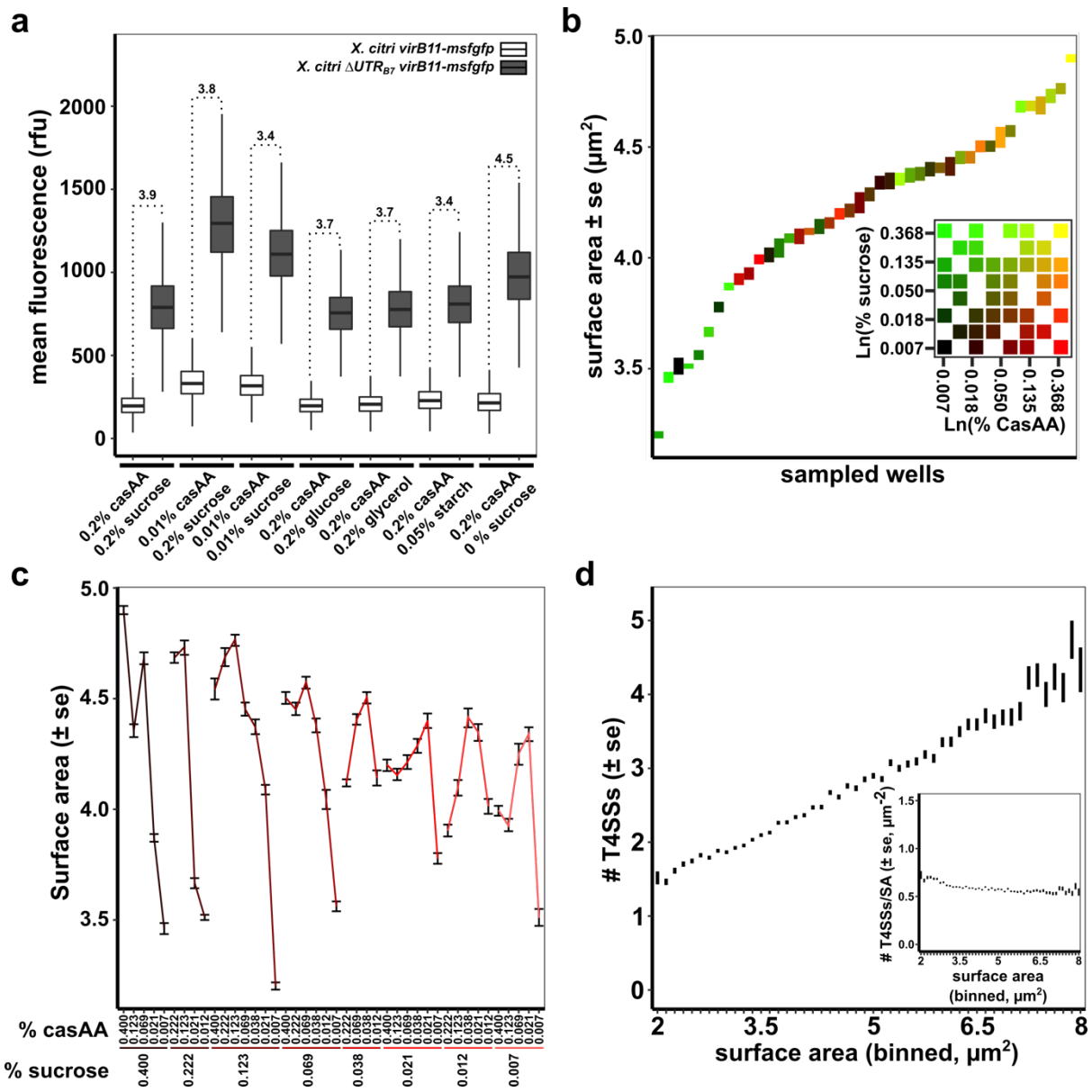

Figure 3: **T4SS production and density in the cell envelope under different nutrient conditions. a)** msfGFP fluorescence levels from *X. citri virB11-msfgfp* and *X. citri Δ5'UTR$_{B7}$ virB11-msfgfp* grown in AB defined media containing either sucrose, glucose, glycerol, starch or no carbohydrate source (0% sucrose) in combination with 0.2% casamino acids (casAA) or in AB defined media containing 0.01% casamino acids with 0.2% or 0.01% sucrose. Mean cytoplasmic msfGFP production from the *X. citri virB11-msfgfp* transcriptional fusion strain in the presence (white boxplots) or absence (grey boxplots) of the *5'UTR$_{B7}$* are represented as Tukey box-and-whisker plots for each media composition with black central line (median), box (first and third quartiles) and whiskers (data within 1.5 interquartile range). On average 6,018 cells were sampled per condition for each strain, with a minimum of 2,162 and a maximum of 16,351 cells from two independent cultures. Note that in this graph, the mean fluorescence (sum of each cell's pixel intensities divided by the number of pixels) is used to take into account differences in cell-sizes between conditions. **b)** Surface area of *X. citri* cells sampled from separate cultures, each culture differing slightly in sucrose and casamino acid concentrations. Cultures are ordered according to the average cell surface area observed for each growth condition. The inset shows the 8x8 matrix range of sucrose and casamino acid concentrations used as described in the text. In both the graph and the inset, each growth condition is colored differently. **c)** Surface area of *X. citri* cells as a function of sucrose and casamino acid concentrations. The data is

750 the same as in panel b but organised with respect to sucrose and casamino acid concentrations and illustrates the link
751 between *X. citri* cell sizes and the culture media. **d)** Average number of T4SSs per cell versus cell surface area from all the
752 cells grown in the different conditions presented in panels b and c. Detection of VirB10-msfGFP foci reveals that the
753 increase of average number of T4SSs correlates with increasing surface area (Pearson correlation r = 0.34, as calculated for
754 all data points). *Inset:* Density of T4SSs in the cell envelope (number of T4SS per surface area, T4SS/SA) versus the surface
755 area. A subtle increase with smaller (and thus more nutrient deprived) cells is observed. Vertical bars in figure b, c and d
756 represent the standard error around the mean (± se). In total 69,412 cells were registered for the data in panels b, c and d.

757

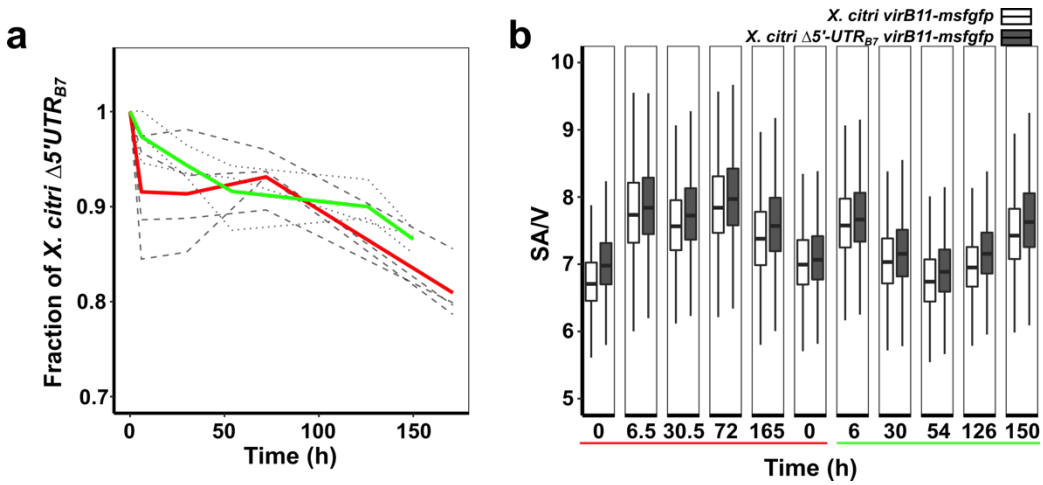

Figure 4: **Overproducing T4SSs leads to a detectable physiological cost for *X. citri*. a**) Co-culture experiment between *X. citri virB11-msfGFP* and X. *citri Δ5'UTR$_{B7}$ virB11-msfGFP* in liquid medium. A decrease in the fraction *X. citri Δ5'UTR$_{B7}$ virB11-msfGFP* cells relative to the wild-type (*X. citri virB11-msfGFP*) cells is observed and becomes pronounced after approximately 1 week incubation. Results from two distinct experiments with 3 (dotted lines and green average) and 4 (dashed lines and red average) separate cultures are shown. In all seven cultures, we observed a significant reduction in the fraction of *X. citri Δ5'UTR$_{B7}$ virB11-msfgfp* cells relative to the wild-type *X. citri virB11-msfgfp* cells at the end-points: 0.87 ± 0.01 (green) and 0.81 ± 0.03 (red). Cells were imaged by fluorescence microscopy and separated by the difference in msfGFP production levels as seen in Figures 2a and 3a. **b**) Comparison of surface area to volume ratios of *X. citri Δ5'UTR$_{B7}$ virB11-msfGFP* and wild-type cells for cells collected at different times for all seven cultures shown in part a. A subtle but consistently smaller average cell size (larger SA/V) in the *Δ5'UTR$_{B7}$* background is observed indicative of a subtle change in physiological state of the cells that can be attributed to the increased production of T4SSs. At each time point an average of 3871 cells were analysed for each culture (minimum: 1061 cells, maximum: 9582 cells).

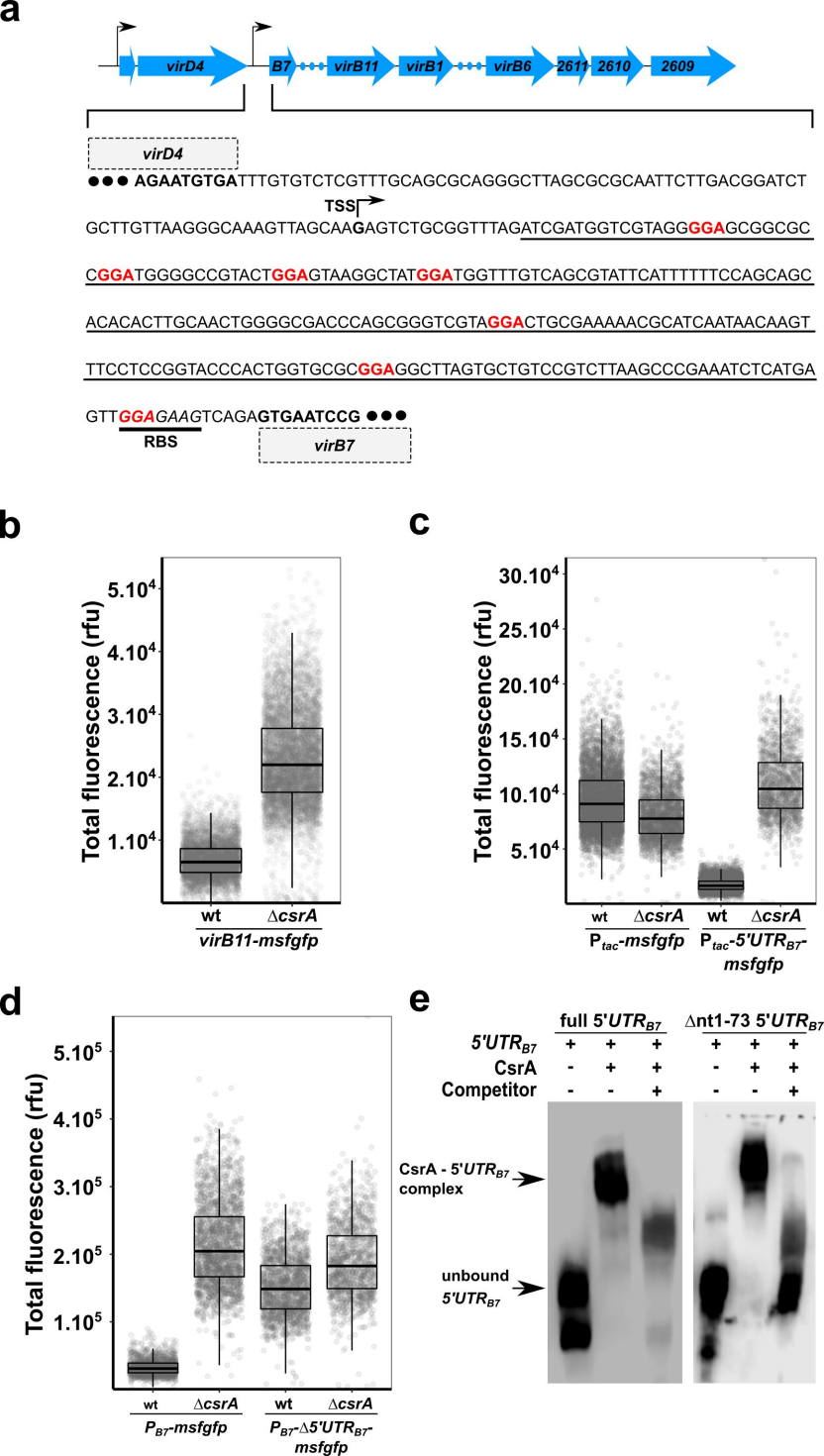
a
virD4
B7
virB11
virB1
virB6
2611
2610
2609
virD4
●●● AGAATGTGATTTGTGTCTCGTTTGCAGCGCAGGGCTTAGCGCGCAATTCTTGACGGATCT
TSS
GCTTGTTAAGGGCAAAGTTAGCAAGAGTCTGCGGTTTAGATCGATGGTCGTAGGGGAGCGGCGC
CGGATGGGGCCGTACTGGAGTAAGGCTATGGATGGTTTGTCAGCGTATTCATTTTTTCCAGCAGC
ACACACTTGCAACTGGGGCGACCCAGCGGGTCGTAGGACTGCGAAAAACGCATCAATAACAAGT
TTCCTCCGGTACCCACTGGTGCGCGGAGGCTTAGTGCTGTCCGTCTTAAGCCCGAAATCTCATGA
GTTGGAGAAGTCAGAGTGAATCCG ●●●
RBS
virB7
b
Total fluorescence (rfu)
5.10^4
4.10^4
3.10^4
2.10^4
1.10^4
wt
ΔcsrA
virB11-msfgfp
c
Total fluorescence (rfu)
30.10^4
25.10^4
20.10^4
15.10^4
10.10^4
5.10^4
wt
ΔcsrA
wt
ΔcsrA
P_tac-msfgfp
P_tac-5'UTR_B7-msfgfp
d
Total fluorescence (rfu)
5.10^5
4.10^5
3.10^5
2.10^5
1.10^5
wt
ΔcsrA
wt
ΔcsrA
P_B7-msfgfp
P_B7-Δ5'UTR_B7-msfgfp
e
full 5'UTR_B7
Δnt1-73 5'UTR_B7
5'UTR_B7
CsrA
Competitor
CsrA - 5'UTR_B7 complex
unbound 5'UTR_B7

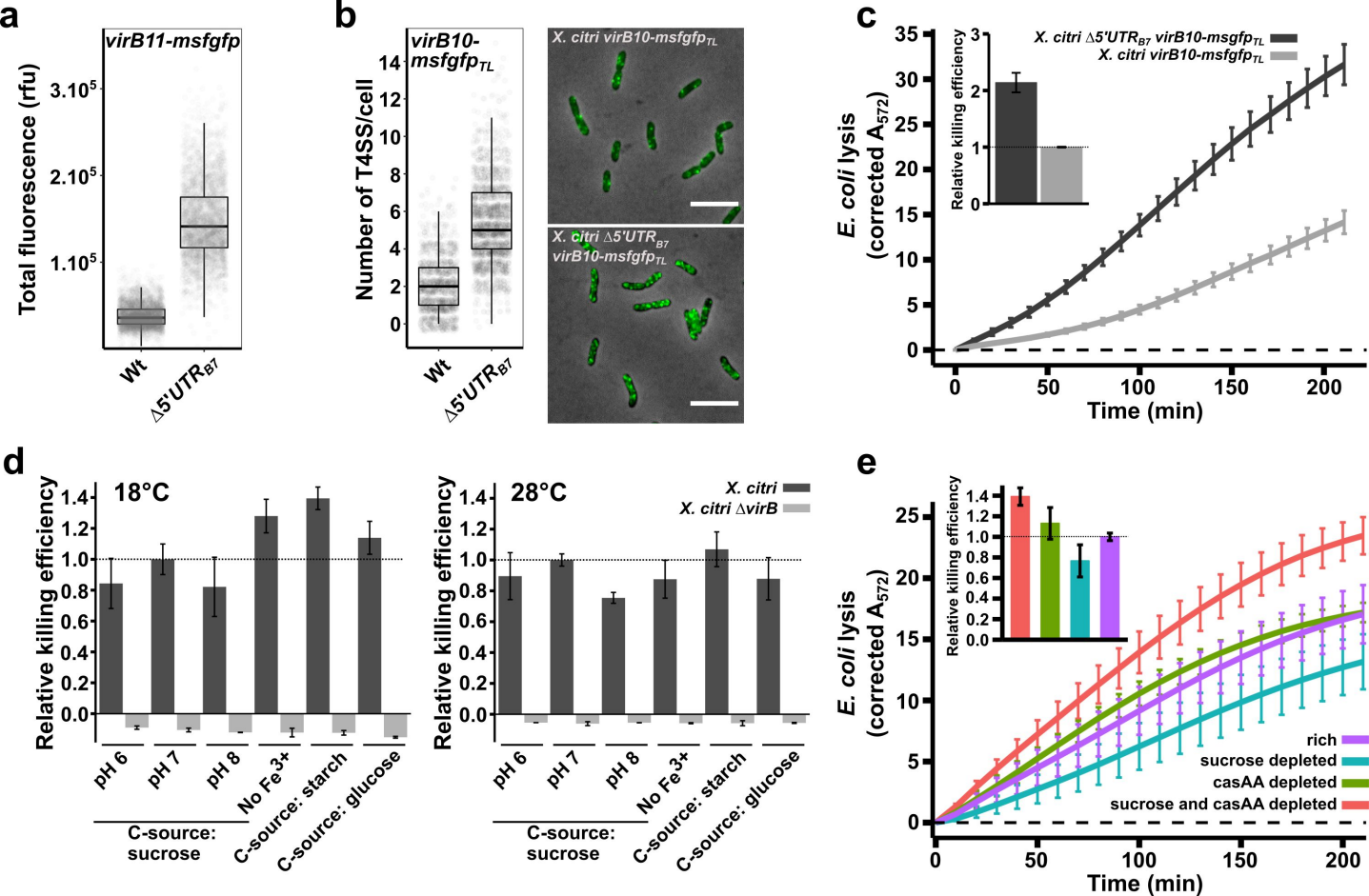
a
virB11-msfgfp
Total fluorescence (rfu)
3.10^5
2.10^5
1.10^5
Wt
Δ5'UTR_B7
b
virB10-msfgfp_TL
Number of T4SS/cell
14
12
10
8
6
4
2
0
Wt
Δ5'UTR_B7
X. citri virB10-msfgfp_TL
X. citri Δ5'UTR_B7 virB10-msfgfp_TL
c
X. citri Δ5'UTR_B7 virB10-msfgfp_TL
X. citri virB10-msfgfp_TL
Relative killing efficiency
E. coli lysis (corrected A_572)
Time (min)
d
18°C
28°C
X. citri
X. citri ΔvirB
Relative killing efficiency
pH 6
pH 7
pH 8
No Fe3+
C-source: starch
C-source: glucose
C-source: sucrose
e
Relative killing efficiency
E. coli lysis (corrected A_572)
Time (min)
rich
sucrose depleted
casAA depleted
sucrose and casAA depleted

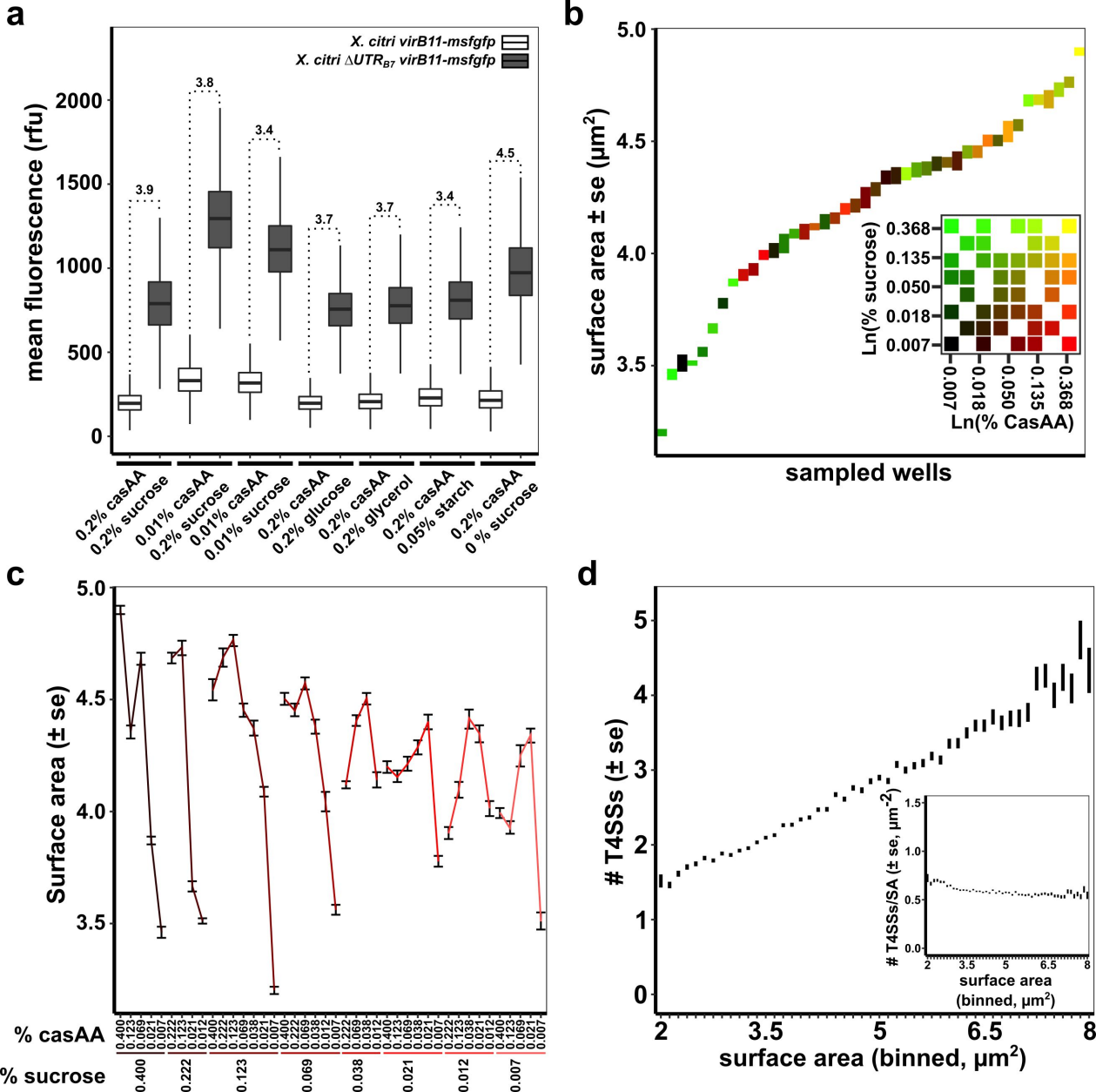
a
X. citri virB11-msfgfp
X. citri ΔUTR$_{B7}$ virB11-msfgfp
mean fluorescence (rfu)
3.9
3.8
3.4
3.7
3.7
3.4
4.5
0.2% casAA 0.2% sucrose
0.01% casAA 0.2% sucrose
0.01% casAA 0.01% sucrose
0.2% casAA 0.2% glucose
0.2% casAA 0.2% glycerol
0.2% casAA 0.05% starch
0.2% casAA 0 % sucrose
b
surface area ± se (μm^2)
sampled wells
Ln(% sucrose)
Ln(% CasAA)
c
Surface area (± se)
% casAA
% sucrose
d
T4SSs (± se)
surface area (binned, μm^2)
T4SSs/SA (± se, μm^{-2})
surface area (binned, μm^2)

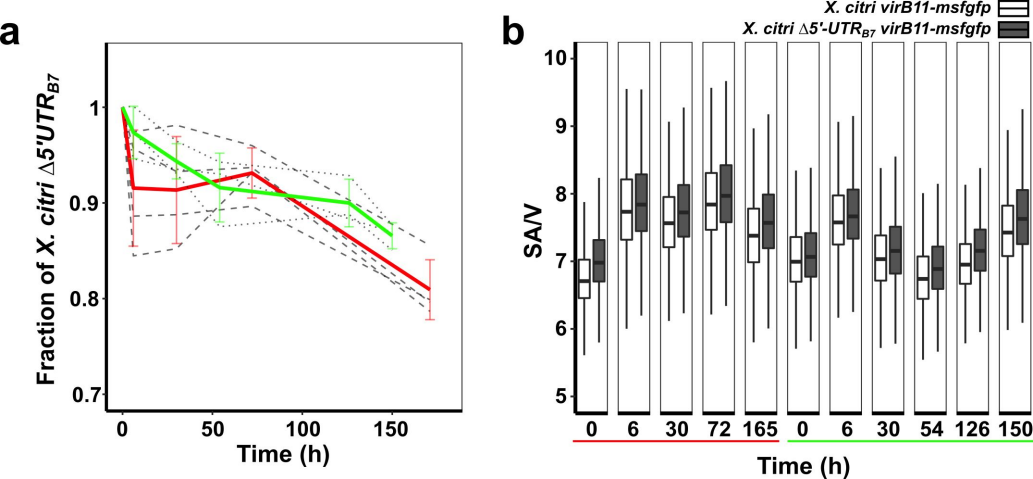
a
Fraction of X. citri Δ5'UTR$_{B7}$
1
0.9
0.8
0.7
0
50
100
150
Time (h)
b
X. citri virB11-msfgfp
X. citri Δ5'-UTR$_{B7}$ virB11-msfgfp
SA/V
10
9
8
7
6
5
0
6
30
72
165
0
6
30
54
126
150
Time (h)